Geology

Rugged crater ejecta as a guide to megaregolith thickness in the southern nearside of the Moon

Thomas W. Thompson, Bruce A. Campbell, Rebecca R. Ghent and B. Ray Hawke

Geology 2009;37;655-658
doi:10.1130/G25565A.1

Rugged crater ejecta as a guide to megaregolith thickness in the southern nearside of the Moon

Thomas W. Thompson[1]*, Bruce A. Campbell[2], Rebecca R. Ghent[3], and B. Ray Hawke[4]
[1]Jet Propulsion Laboratory, California Institute of Technology, 4800 Oak Grove Drive, Mail-Stop 300-227, Pasadena, California 91109-8099, USA
[2]National Air and Space Museum, Center for Earth and Planetary Studies, Smithsonian Institution, MRC 315, P.O. Box 37012, Washington, D.C. 20013-7012, USA
[3]University of Toronto, Department of Geology, 22 Russell Street, Toronto, Ontario M5S 3B1, Canada
[4]Hawai'i Institute of Geophysics and Planetology, University of Hawai'i, 1680 East-West Road, Honolulu, Hawaii 96822, USA

ABSTRACT

The southern highlands of the Moon comprise superposed ejecta layers, individually as thick as a few kilometers, from the major basins. Smaller (1–16-km-diameter) impact craters that penetrate this layered megaregolith and excavate material from depth have radar properties that provide insight into the variability of megaregolith thickness above a postulated basement of large crustal blocks. We observe a significant difference in the population of radar-bright craters, 1–16 km and larger in diameter, between regions of the southeastern nearside highlands north and south of ~lat 48°S. There are about one-third more radar-bright craters north of this line than to the south, broadly coincident with the mapped boundary between southern deposits mapped as pre-Nectarian age and those of Nectarian–Imbrian age to the north. The radar-bright crater population is consistent with a megaregolith thickness of ~1.5 km in the north and ~2.5 km in the south, a difference we attribute to South Pole–Aitken basin ejecta.

INTRODUCTION

Current models hypothesize that the lunar highlands formed as a feldspar-rich crust from an early magma ocean after the formation of the Moon 4.6 Ga ago. This early crust was substantially reworked during the heavy bombardment, up until the end of the terminal cataclysm ca. 3.8 Ga ago. Much of the upper few kilometers was broken up and distributed as fragmented and chaotically mixed debris by basin-forming impacts. Subsequent cratering events continued to develop the fragmental layer or megaregolith, and still smaller impacts over time created several meters of fine-grained surface regolith. Several researchers (e.g., Hartmann, 1973; Head, 1976) defined megaregolith as the fragmental layer of impact crater and basin ejecta above fractured bedrock, a definition we adopt here. Head (1976) used geologic and seismic data to suggest that the megaregolith is typically 2–3 km in thickness.

Oberbeck and Morrison (1976) suggested, prior to recognition of the scale of the South Pole–Aitken basin, that some areas of the southern highlands may be almost unmantled by basin debris surges and thus represent in situ ancient materials. Instead, the southern nearside highlands are composed of deep material excavated by the enormous South Pole–Aitken basin and several other old, large basins (e.g., Australe, Mutus-Vlacq), overprinted by younger and thinner material from later basins like Imbrium, Nectaris, and Nubium (Wilhelms, 1987; Wilhelms et al., 1979). The importance of the south polar region for potential future exploration motivates renewed interest in the detailed structure of the highlands megaregolith and the degree to which particular basins contribute to the upper layers of material at any particular landing site (e.g., Petro and Pieters, 2004, 2006).

One source of information on highland megaregolith properties comes from the distribution of blocky (meter-sized) ejecta, detected by Earth-based radar, surrounding smaller (1–16-km-diameter) impact craters (Thompson et al., 1979). As craters on the Moon excavate material from depths of about one-tenth their diameter (Pike, 1977, 1980), they provide a means for probing the Moon's upper crust. Radar backscatter measurements, particularly at longer wavelengths, can directly sense the abundance of meter-sized rocks within the upper several meters of the regolith. Previous surveys based on radar images with 5–10 km resolution and infrared eclipse temperature maps with resolution of 14–30 km showed significant differences between the proximal ejecta of radar-bright craters formed in the basaltic maria, where competent bedrock is below a shallow regolith, and those formed in the highlands, where radar-bright craters are sparse because large blocks are mixed in a greater thickness of pulverized debris (Thompson et al., 1974, 1979, 1980). The shift from smaller highland craters with minimal radar-bright ejecta to larger craters with rugged near-rim deposits occurs at ~12 km diameter, implying an average megaregolith thickness of 1.2 km (Thompson et al., 1979).

In this paper, we use new 70-cm-wavelength radar images of the Moon to study the variations in crater ejecta blankets within a large region of the southern highlands, down to craters of 1–2 km diameter. The 70-cm-wavelength data used here were obtained by transmitting a circular-polarized signal from the Arecibo Observatory and receiving echoes from the Moon, in both senses of circular polarization, at the Green Bank Telescope (Campbell et al., 2007). Spatial resolution of the images after focused processing and multilook averaging is 400–500 m per pixel. Echoes in the same sense of circular polarization (SC) as that transmitted are attributed to diffuse scattering by rocks, of 10 cm and larger diameter, at the surface and buried within the probing depth of the radar signal. In the low-loss materials of the lunar highlands, the probing depth at 70 cm wavelength may be as great as 40 m (Campbell and Hawke, 2005). The ratio of echoes in the SC mode to those in the opposite-sense circular (OC) polarization, termed the circular polarization ratio (CPR), is useful in highlighting subtle changes in rock abundance. The next section presents an analysis of craters with radar-bright ejecta across the highlands, and compares these results with the population of craters with radar-dark distal ejecta haloes (Ghent et al., 2005, 2008; Thompson et al., 2006). The last section interprets the radar-bright crater abundance across the highlands in terms of regional variations in megaregolith thickness linked with the major basins.

REGIONAL VARIATIONS IN CRATER PROPERTIES

Our study region encompasses a part of the central and southeastern highlands that is relatively unaffected by the distal deposits of Orientale basin, allowing a view of terrain from the southern mare-filled basins (Nectaris to the east and Nubium to the west) to near the South Pole (5°W–56°E, 24°S–70°S) (Fig. 1). We identified the radar-bright craters in this region with diameters of 1–16 km (i.e., those craters with radar-bright ejecta within about one crater radius of the rim) as indicators of relatively younger impacts that excavated substantial blocky material (Fig. 2). For comparison, we counted radar-bright craters in

*E-mail: Thomas.W.Thompson@jpl.nasa.gov.

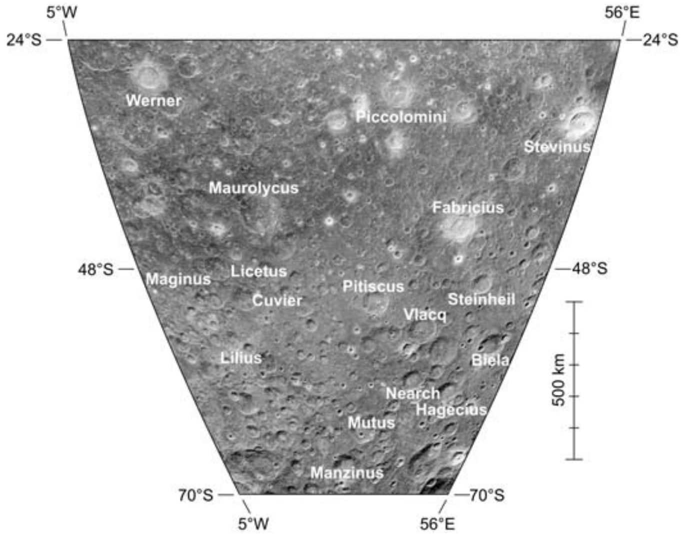

Figure 1. Southern highlands, 70 cm radar view. Image area is 5°W–56°E, 24–70°S in sinusoidal equal-area map projection. These data were obtained by transmitting circular-polarized signal from Arecibo Observatory and receiving echoes from the Moon, at Green Bank Telescope (Campbell et al., 2007) in the same sense of circular polarization (SC) as those transmitted. These radar echoes are attributed to diffuse scattering by rocks, of 10 cm and larger diameter, at surface and buried within probing depth of radar signal, which may be as great as 40 m. Spatial resolution of the images is 400–500 m per pixel.

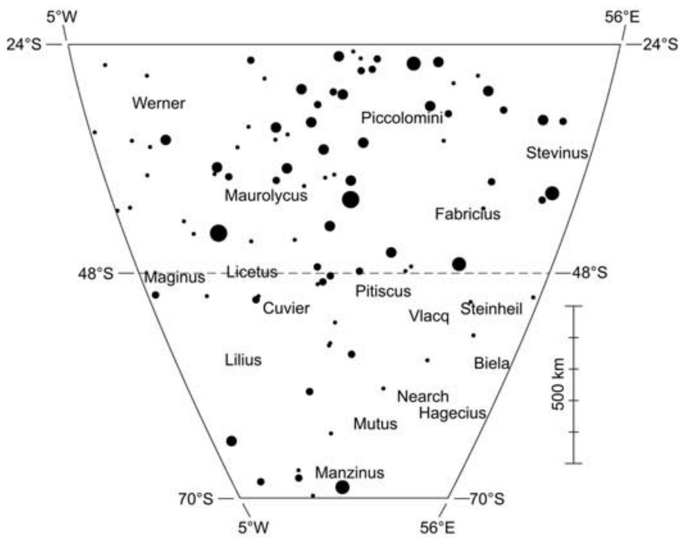

Figure 2. Locations of craters with 70 cm radar-bright ejecta; relative sizes are indicated by diameter of plot symbol for highlands area shown in Figure 1. Note that there are more radar-bright craters north of 48°S than there are south of this latitude.

Mare Humorum, where the target terrain is kilometers-thick basalt lava flows (Table 1).

We also mapped all craters larger than 2–4 km in diameter with radar-dark haloes, which previous work has shown to be a rock-poor distal facies ubiquitous among late Imbrian and younger craters (Ghent et al., 2005, 2008). Figure 3 shows that there is a relatively uniform distribution of craters with such haloes across the highlands study region, consistent with earlier results that map all of these terrains as early Imbrian or older (i.e., older than the typical halo retention age). We therefore expect a similar distribution of craters with radar-bright, near-rim ejecta across

TABLE 1. NUMBER OF RADAR-BRIGHT CRATERS PER 10^6 km^2

Value	Study region		
	Mare Humorum	Highlands 24°S–48°S	Highlands 48°S–70°S
Area (10^6 km^2)	0.072	1.08	0.63
Number of craters counted			
1–2 km diameter	138 ± 12	11 ± 3.2	5 ± 2.7
2–4 km diameter	166 ± 13	13 ± 3.5	7 ± 3.0
4–8 km diameter	97 ± 10	17 ± 3.9	10 ± 3.6
8–16 km diameter	28 ± 5.3	24 ± 4.7	7 ± 3.0

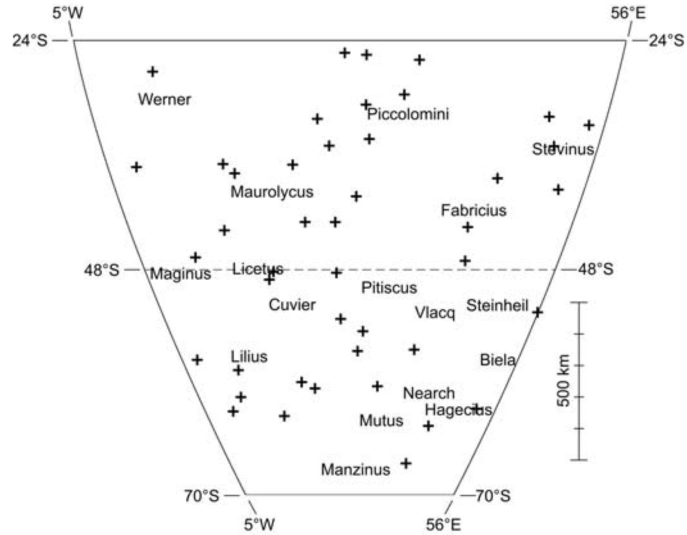

Figure 3. Locations of craters with radar-dark haloes for highlands area shown in Figure 1. Note relatively uniform distribution of craters with radar-dark haloes across study area, consistent with our expectation of no difference in the population of late Imbrian and younger craters in this region (Ghent et al., 2005).

the region, since these deposits likewise survive from about the Imbrian period. In contrast to this expectation, however, there is a marked difference in the population of smaller radar-bright craters from north to south across a line at ~48°S.

Relative size-frequency distributions for small, radar-bright craters in Mare Humorum and the southern highlands are compared with those of previous studies (Fig. 4) (Wilhelms et al., 1978; Thompson et al., 1980; Crater Analysis Group, 1979). There are five sets of data: one each for the previous studies, and new relative crater frequencies for Mare Humorum and the northern and southern lunar highlands. The relative crater frequency for Imbrian period and younger craters cited by Wilhelms et al. (1978) has a slope of ~0.0125, indicating a production population (which would have a curve proportional to crater diameter squared in a cumulative size-frequency distribution). Similarly, the relative frequencies of infrared-bright and radar-bright craters with diameters of 20–30 km cited in Thompson et al. (1980) have a constant value of ~0.0125, indicating that these infrared-bright and radar-bright craters are Imbrian and younger. For the larger (4–16 km diameter) radar-bright craters in Mare Humorum, the relative crater frequency also has a constant value of ~0.0125, indicative of a production population. The smaller mare craters (1–4 km diameter) are better fit by an inverse-cube behavior in a cumulative frequency distribution. This change in slope could result either from a loss of detection because of image resolution, or because the radar enhancements associated with these smaller craters disappear on time scales less than the age of the mare units.

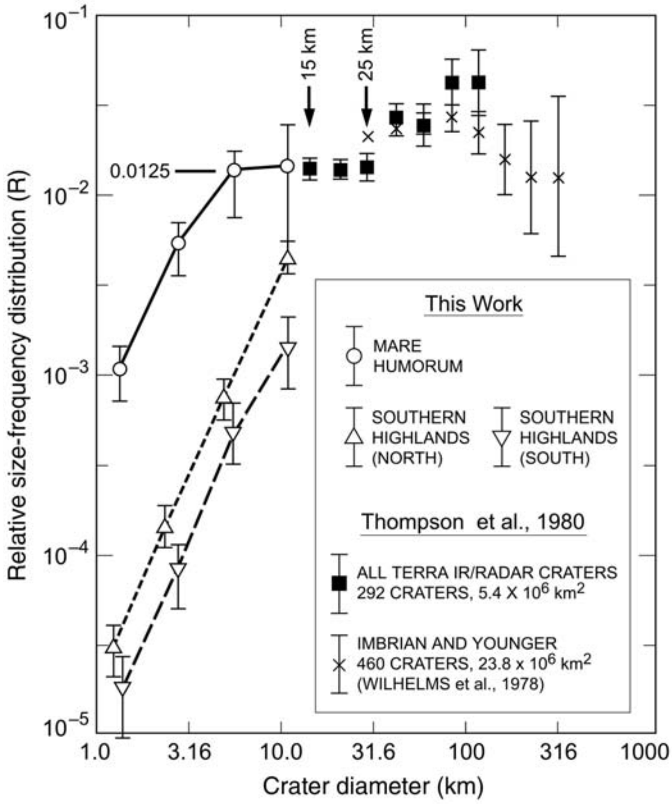

Figure 4. Relative size-frequency distributions of radar-bright Mare Humorum and southern highland terra craters based on new 70 cm data. Also shown are previous global mare and terra infrared-bright and radar-bright craters for size ranges of 16–100 km from Thompson et al. (1980) as well as the Imbrian and younger craters for sizes of 20–316 km reported by Wilhelms et al. (1978). Note that the relative crater frequency of radar-bright craters in Mare Humorum with 4–16 km diameters is ~0.0125. When the northern and southern radar-bright crater frequencies are extrapolated back to 0.0125, the crater diameters are 15 km and 25 km, respectively. IR—infrared.

IMPLICATIONS FOR A THICKER MEGAREGOLITH IN THE SOUTH

Smaller (1–16-km-diameter) radar-bright craters in the northern highlands are less abundant than in the maria, differing by about a factor of 10 at diameters of 1–4 km. The relative frequency of radar-bright craters in the highlands south of 48°S exhibits a similar size-frequency dependence, but they occur about one-third less frequently on average than radar-bright craters in the north. When the northern radar-bright crater frequencies are extrapolated back to a relative value of 0.0125, the crater diameter is 15 km. As craters excavate to a depth of about one-tenth of their diameters, this implies a megaregolith thickness of 1.5 km in the north, consistent with the result of Thompson et al. (1980) for typical lunar highlands. Similarly, when the southern radar-bright crater frequencies are extrapolated back to 0.0125, the crater diameter is 25 km, implying a megaregolith thickness of 2.5 km. This change in thickness with latitude agrees with Clementine topographic data, which show that the southern nearside highlands increase in elevation, relative to the mean lunar radius, from an average of –1 km north of 48°S to an average near 0 km south of 48°S toward the South Pole–Aitken basin (http://www.lpi.usra.edu/lunar/missions/clementine/images/).

Differences between the radar-bright mare and terra craters with diameters of 1–16 km result from the competence of the target materials. Mare craters of this size have been formed in solid basalts to produce abundant meter-sized ejecta that create 70 cm radar echo enhancements. For terra craters north of 48°S compared with those south of 48°S, there is a higher probability that they will penetrate the thinner megaregolith and tap into the underlying consolidated bedrock. There is also the possibility that the thinner megaregolith has more abundant buried large (hundreds of meters in size) blocks that in turn provide for more consolidated crater ejecta that survives longer. We conclude that the megaregolith thickness increases on average by ~1 km across a line near 48°S, a result consistent with Clementine altimetry and attributed here to South Pole–Aitken basin ejecta. This result is important as a guide to the general stratigraphy and near-surface properties of potential landing sites in the south polar region, and provides a constraint on models for large-scale ejecta distribution on the Moon.

ACKNOWLEDGMENTS

We thank the staff at Cornell University, the Arecibo Observatory, and the Robert C. Byrd Green Bank Telescope for invaluable assistance in collecting the new 70 cm lunar radar data. The Arecibo Observatory is part of the National Astronomy and Ionosphere Center, which is operated by Cornell University under a cooperative agreement with the National Science Foundation (NSF) and with support from the National Aeronautics and Space Administration (NASA). The Green Bank Telescope is part of the National Radio Astronomy Observatory, a facility of the NSF operated under cooperative agreement by Associated Universities, Inc. We thank James W. (Jim) Head and Noah E. Petro for their insightful review comments. This work was supported in part by grants from the NASA Planetary Geology and Geophysics Program. Research by Thompson was carried out at the Jet Propulsion Laboratory, California Institute of Technology, and was sponsored by NASA.

REFERENCES CITED

Campbell, B.A., and Hawke, B.R., 2005, Radar mapping of lunar cryptomaria east of Orientale basin: Journal of Geophysical Research, v. 110, no. E9, E09002, doi: 10.1029/2005JE002425.

Campbell, B.A., Campbell, D.B., Margot, J.L., Ghent, R.R., Nolan, M., Chandler, J., Carter, L.M., and Stacy, N.J.S., 2007, Focused 70-cm radar mapping of the Moon: IEEE Transactions on Geoscience and Remote Sensing, v. 45, p. 4032–4042, doi: 10.1109/TGRS.2007.906582.

Crater Analysis Group, 1979, Standard techniques for presentation and analysis of crater size-frequency distributions: Icarus, v. 37, p. 467–474, doi: 10.1016/0019-1035(79)90009-5.

Ghent, R.R., Leverington, D.W., Campbell, B.A., Hawke, B.R., and Campbell, D.B., 2005, Earth-based observations of radar-dark crater haloes on the Moon: Implications for regolith properties: Journal of Geophysical Research, v. 110, no. E2, E02005, doi: 10.1029/2004JE002366.

Ghent, R.R., Campbell, B.A., Hawke, B.R., and Campbell, D.B., 2008, Earth-based radar data reveal extended deposits of the Moon's Orientale basin: Geology, v. 36, p. 343–346, doi: 10.1130/G24325A.1.

Hartmann, W.K., 1973, Ancient lunar megaregolith and subsurface structure: Icarus, v. 18, p. 634–639.

Head, J.W., 1976, The significance of substrate characteristics in determining morphology and morphometry of lunar craters, *in* Proceedings, Lunar Science Conference, 7th, Houston, Texas, v. 3, p. 2913–2929.

Oberbeck, V.R., and Morrison, R.H., 1976, Candidate areas for in situ ancient lunar areas, *in* Proceedings, Lunar Science Conference, 7th, Houston, Texas, v. 3, p. 2983–3005.

Petro, N.E., and Pieters, C.M., 2004, Surviving the heavy bombardment: Ancient material at the surface of South Pole-Aitken basin: Journal of Geophysical Research, v. 109, E06004, doi: 10.1029/2003JE002182.

Petro, N.E., and Pieters, C.M., 2006, Modeling the provenance of the Apollo 16 regolith: Journal of Geophysical Research, v. 111, E09005, doi: 10.1029/2005JE002559.

Pike, R.J., 1977, Size dependence in the shape of fresh impact craters on the Moon, *in* Roddy, D.J., et al., eds., Impact and explosion cratering: New York, Pergamon Press, p. 489–509.

Pike, R.J., 1980, Geometric interpretation of lunar craters: U.S. Geological Survey Professional Paper 1046-C, 77 p.

Thompson, T.W., Masursky, H., Shorthill, R., Tyler, G.L., and Zisk, S.H., 1974, A comparison of infrared, radar, and geologic mapping of lunar craters: The Moon, v. 10, p. 87–117, doi: 10.1007/BF00562019.

Thompson, T.W., Roberts, W.J., Hartmann, W.K., Shorthill, R.W., and Zisk, S.H., 1979, Blocky craters: Implications about the lunar megaregolith: The Moon and the Planets, v. 21, p. 319–342, doi: 10.1007/BF00897360.

Thompson, T.W., Cutts, J.A., Shorthill, R.W., and Zisk, S.H., 1980, Infrared and radar signatures of lunar craters: Implications about crater evolution, *in* Papike, J.J., and Merrill, R.B., eds., Proceedings, Conference on the Lunar Highlands Crust, November 1979: Houston, Texas, Lunar and Planetary Institute, p. 483–499.
Thompson, T.W., Campbell, B.A., Ghent, R.R., Hawke, B.R., and Leverington, D.W., 2006, Radar probing of planetary regoliths: An example from the northern rim of Imbrium basin: Journal of Geophysical Research, v. 111, E06S14, doi: 10.1029/2005JE002566.
Wilhelms, D.E., 1987, The geologic history of the Moon: U.S. Geological Survey Professional Paper 1348, 302 p.
Wilhelms, D.E., Overbeck, V.R., and Aggarwal, H.R., 1978, Size-frequency distribution of primary and secondary lunar craters *in* Proceedings, Lunar and Planetary Science Conference, 9th, Houston, Texas, p. 3735–3762.
Wilhelms, D.E., Howard, K.A., and Wilshire, H.G., 1979, Geologic map of the south side of the Moon: U.S. Geological Survey Map I-1162, scale 1:5,000,000.

Manuscript received 23 October 2008
Revised manuscript received 10 March 2009
Manuscript accepted 18 March 2009

Printed in USA

ERRATUM

Multiphase development of the Atacama Planation Surface recorded by cosmogenic ^{3}He exposure ages: Implications for uplift and Cenozoic climate change in western South America

Laura A. Evenstar, Adrian J. Hartley, Finlay M. Stuart, Anne E. Mather, Clive M. Rice, Guillermo Chong
Geology, v. 37, p .27–30 (January 2009)

Table 1 in Evenstar et al. has an error in the "^{3}He" column. The correct table is given here.

TABLE 1. HELIUM CONCENTRATIONS AND MODELED EXPOSURE AGES IN PYROXENE AND AMPHIBOLE FROM BOULDERS FROM AROMA AREA (NORTHERN CHILE) AND THE TANA LAVA

Site	Sample	Mineral	^{3}He (10^8 atoms/g)	Exposure age (Ma)
A	11/24	Pyroxene	2.2 ± 0.1	1.3
	12/24	Pyroxene	2.1 ± 0.1	1.2
	14/24	Pyroxene	2.1 ± 0.1	1.3
B	22/24	Pyroxene	12.9 ± 0.5	7.3
	23/24	Amphibole	12.1 ± 0.3	6.8
	24/24	Pyroxene	12.6 ± 0.4	7.1
C	04/26	Pyroxene	17.9 ± 0.5	10.1
D	03/02a	Amphibole	27.5 ± 0.4	14.6
	03/02b	Amphibole	26.9 ± 0.5	14.8
	05/02	Amphibole	30 ± 0.4	16.5
E	09/02	Pyroxene	5.7 ± 0.1	2.6
F	11/26	Pyroxene	7.5 ± 0.2	3.0
	13/26	Pyroxene	7.1 ± 0.2	2.8
	15/26	Pyroxene	6.6 ± 0.2	2.6
G	21/26	Pyroxene	31.9 ± 0.9	14.8
	22/26	Pyroxene-amphibole	31.8 ± 0.9	14.7
	23/26	Pyroxene	42.4 ± 0.3	22.00
H	04/27	Pyroxene-amphibole	26.1 ± 0.8	6.8
	05/27	Pyroxene	12.2 ± 0.3	3.0
	06/27	Amphibole	28.7 ± 0.7	7.6
I	12/02	Pyroxene	10.5 ± 0.2	2.6
J	12/27	Pyroxene	20.8 ± 0.4	5.2
	13/27	Pyroxene	20.8 ± 0.6	5.2
Tana lava	07/04	Pyroxene	0	0.0077